Flexural ductility of HSC members

A. A. Maghsoudi[†] and H. Akbarzadeh Bengar[‡]

Civil Engineering Department, Kerman University, Kerman, Iran

Abstract.   In seismic areas, ductility is an important factor in design of high strength concrete (HSC) members under flexure. A number of twelve HSC beams with different percentage of ρ & ρ' were cast and incrementally loaded under bending. The effect of ρ' on ductility of members were investigated both qualitatively and quantitatively. During the test, the strain on the concrete middle faces, on the tension and compression bars, and also the deflection at different points of the span length were measured up to failure. Based on the obtained results, the serviceability and ultimate behavior, and especially the ductility of the HSC members are more deeply reviewed. Also a comparison between theoretical and experimental results are reported here.

Keywords: curvature and displacement ductility; HSC members; serviceability.

1. Introduction

Advances in concrete technology in many countries have now made practical use of concrete with strengths up to 90 MPa. These concretes, with very high compressive strength, can result in less ductile responses of structural members. It has been found that flexural ductility, in terms of maximum curvatures attainable, may be smaller in high-strength concrete (HSC) beams (ACI Committee 363 1992, Ozbakkaloglu and Saatcioglu 2004, Ahmad and Barker 1991, Ashour and Wafa 1993).

HSC provides a better solution to reduce sizes and weights of concrete structural element (ACI Committee 363 1992, Nilson 1987, Swamy 1987). This reduction in cross section reflects on the reduced moment of inertia, I, of the members, which necessitates the investigation of the corresponding deflection under the service load. The value of I (for both NSC and HSC) changes along the beam span from a maximum value of I_g for uncracked (gross) section to a minimum value of I_{cr} for the fully cracked section. The variation of I along the span length makes the deflection calculation not only lengthy and tedious but also difficult to achieve accurately. Hence, in a cracked member, to provide a smooth continuous transition between I_g and I_{cr}, over the entire length of a simply supported beam, ACI 318-2005 (ACI Committee 318 2005) recommends the following expression for the calculation of the effective moment of inertia:

---
† Assistant Professor, Corresponding author, E-mail: maghsoudi.a.a@mail.uk.ac.ir
‡ Engineer, E-mail: h_akbarzadeh_b@yahoo.com

$$I_e = \left(\frac{M_{cr}}{M_a}\right)^3 I_g + \left[1 - \left(\frac{M_{cr}}{M_a}\right)^3\right] I_{cr} \qquad (1)$$

where

M_a = maximum moment in a member at the stage that deflection is computed.

M_{cr} = cracking moment of beam.

A few limited studies have been made for HSC (Khuntia and Ghosh 2004, Ashour *et al.* 2000, Leslie *et al.* 1976, Ashour 2000). Ashour (2000) believes that the utilization of HSC impacts the parameters involved in the deflection calculations. This includes concrete modulus of elasticity and cracked moment of inertia. He modified the above Eq. (1) for the effective moment of inertia. Ashour (2000) tested nine reinforced HSC beams to investigate the effect of concrete compressive strength and flexural tensile reinforced ratio on load-deflection behavior and displacement ductility of cracked rectangular reinforced concrete beams. He concluded that, for the same concrete strength, the displacement ductility, μ_d, decreases as the ratio ρ/ρ_b increases. Shin *et al.* (1989) also concluded that, the variation of μ_d as a function of ρ for different f_c' is to decrease μ_d as ρ increases. Tsong *et al.* (1989) conducted the tests for amelioration of stirrup and compression reinforcement on the ductility of reinforced HSC beam and they were concluded that, the ductility of HSC beam can be well improved by adding the compression steel, and the more it content, the better it will be. Moreover, it is more advantageous for the ductility to choose the compressive reinforcement of larger diameter and closely spaced stirrup.

The object of this research is to investigate the effect of ρ and ρ' both qualitatively and quantitatively on the ductility and deflection of HSC beams. The experimental and theoretical (recommended by ACI & CSA Codes) ductility values are compared. Also an experimental and theoretical comparison were made for the beams under service loads.
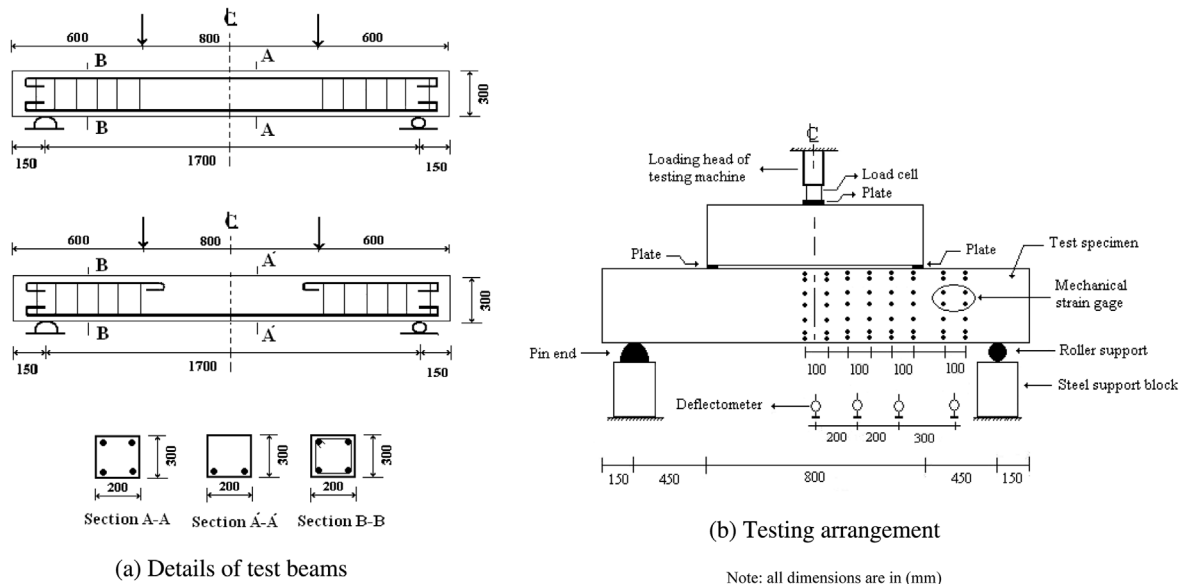

(a) Details of test beams

(b) Testing arrangement

Note: all dimensions are in (mm)

Fig. 1 Details of test beams and testing arrangement

2. Experimental program

2.1 Test specimens

Twelve HSC reinforced beams were cast and tested in this investigation. Fig. 1 shows the beam dimension, reinforcement details and loading arrangement. Five beams were singly reinforced and the other seven doubly reinforced. Shear reinforcement was provided along the beam length except in the constant moment zone. For all the beams a constant value of 1.8 was considered as the ratio of shear span to the effective depth (a/d) to check its validity for avoiding shear failur. The variables were the flexural tensile and compression reinforcement ratio ρ and ρ'. Table 1 presents the detailed testing program. Thus for the beam numbers B1-B5 and BC1-BC7, letter B stands for singly reinforced beams and the letters BC represent the beams with compression bars, and number 1 to 7 indicate the variable amount of ρ and ρ'. To investigate, the effect of quantity of tensile bars and qualitative effect of compressive bars, the beams were divided into two groups. In group 1; the beams BC1-BC4 & BC7, and B1-B5 were considered, and in group 2; to illustrate the qualitatively effect of compressive bars, the beams B5 & BC5-BC7 were considered. For all the doubly reinforced beams in group 1; the percentage of tensile bars (ρ) were variable and the amount of the percentage of compressive bars (ρ') in each beam was chosen half the amount of ρ (except beam BC1). In group 2; the percentage of tensile bars (ρ) were considered to be constant whereas, the amount of (ρ') were variable.

Table 1 Testing program detail of the tested beams

Beam no.	f'_c (MPa)	f_y (MPa)	d (mm)	d' (mm)	A_s	ρ (%)	A'_s	ρ' (%)	$^*\varepsilon'_s$ ($\times 10^{-6}$)	ε_{su}	f_{su} (MPa)
BC1	56.31	398	254	42	2Φ14	0.61	2Φ14	0.61	138	0.0350	623.7
B1	69.50	398	254	-	2Φ14	0.61	-	-	-	0.0274	573.0
BC2	63.48	401	250	47	2Φ20	1.25	2Φ14	0.61	679	0.0184	500.0
B2	70.50	401	250	-	2Φ20	1.25	-	-	-	0.0184	500.0
BC3	63.21	373	251	42	4Φ18	2.03	2Φ14+1Φ18	1.01	664	0.0180	497.0
B3	70.80	373	251	-	4Φ18	2.03	-	-	-	0.0148	469.3
BC4	71.45	401	250	47	4Φ20	2.51	2Φ14+1Φ20	1.24	698	0.0174	491.8
B4	72.80	401	250	-	4Φ20	2.51	-	-	-	0.0089	400.0
BC5	72.98	404	256	40	4Φ28	4.81	2Φ14	0.61	957	0.0113	438.8
B5	71.00	404	256	-	4Φ28	4.81	-	-	-	0.0020	400.0
BC6	73.42	404	256	40	4Φ28	4.81	2Φ20	1.23	1068	0.0117	442.4
BC7	72.98	404	256	40	4Φ28	4.81	2Φ28	2.41	1089	0.0125	449.3

$^*\varepsilon'_s$ is the compressive steel strain at time of yielding of tensile steel.

Table 2 Concrete mix proportion

Cement (kg/m^3)	Microsilica (kg/m^3)	Coarse agg. (kg/m^3)	Fine agg. (kg/m^3)	Super-plasticizer (kg/m^3)	W/C ratio
649	55	723	646	11	0.32

2.2 Materials

Locally available deformed bars were used as flexural and shear reinforcement. The bars were tested and tested values of f_y are shown in Table 1. The concrete mix design is shown in Table 2 and the concrete compressive strength f_c' for each beam is shown in Table 1. All beams and control specimens were cast and cured under similar conditions. The beams and specimens were kept covered under polyethylene sheets for 28 days until 24 hours before testing.

2.3 Test procedure

All the twelve beams were tested under simply supported condition and were subjected to two-point loads, as shown in Fig. 1. The distance between the two loading point was kept constant at 800 mm. The deflections were measured at different points as shown in Fig. 1, but only the midspan deflections are reported here. Strains in the tension and compression steel were measured by electrical strain gages. The demec points (stainless steel disc) were fixed, with 20 station for each single vertical axis, for measuring the concrete strains (see Fig. 1). Again only the midspan concrete strain is reported herein. The load was applied by means of a 1400 kN hydraulic testing machine. The load was applied in 20 to 25 increments up to failure. At the end of each load increment, observations, measurements, crack development, and propagation on the beam surfaces were recorded.

Fig. 2 Crack propagation and failure of the beams under load

Table 3 Experimental and theoretical bending moment of tested beams

Beam no.	$M_{u(exp)}$ kN·m	$M_{y(exp)}$ kN·m	$M_{cr(exp)}$ kN·m	$M_{u(th\text{-}ACI)}$ kN·m	$M_{u(th\text{-}CSA)}$ kN·m	$M_{cr(th\text{-}ACI)}$ kN·m	$M_{cr(th\text{-}CSA)}$ kN·m
BC1	44.54	23.96	9.41	32.00	32.20	13.96	6.75
B1	36.93	18.39	9.40	30.37	30.29	15.51	7.50
BC2	71.00	47.334	11.99	60.87	60.69	14.82	7.17
B2	74.74	59.60	12.49	60.47	59.75	15.62	7.56
BC3	112.75	79.97	12.93	83.58	87.77	14.79	7.15
B3	93.59	75.84	7.63	89.44	88.58	15.65	7.57
BC4	127.75	93.49	8.09	115.79	114.84	15.72	7.61
B4	122.28	96.23	7.20	115.96	114.44	15.87	7.68
BC5	212.86	189.63	15.14	219.50	215.50	15.98	7.73
B5	202.63	197.33	10.73	213.76	207.88	15.67	7.58
BC6	232.43	184.49	11.03	222.10	219.24	15.94	7.71
BC7	233.00	188.16	12.05	224.27	222.31	15.89	7.69

3. Test results and discussions

The beams were all designed to fail in flexure. All beams exhibited vertical flexural cracks in the constant moment region before final failure of the beams due to crushing of concrete. Fig. 2 shows the crack propagation under the load.

Table 3 presents the experimental and theoretical (ACI & CSA) cracking, yielding and ultimate moments of the test specimens. The experimental cracking moment, $M_{cr(exp)}$, corresponds to the moment at which the moment-curvature curve deviates from its initial slope. The experimental yielding moment, $M_{y(exp)}$, corresponds to the moment at the beginning of the yielding flat plateau in the moment-curvature curve (it is remained that, for different bars diameter used here, tensile tests were performed with a universal testing machine which was able to draw the stress-strain curves and their values of f_y are shown in Table 1, the commencements of yielding of steel reinforcement obtained were checked with the moment-curvature diagrams, and it was confirmed that almost for all cases, the two commencement of yielding of steel reinforcement were coincide with each other). The experimental ultimate moment, $M_{u(exp)}$, is the moment when the ultimate load was reached during testing. The results obtained show that the experimental moments are higher than the theoretical values. A comparison between the two Codes (ACI & CSA) for the theoretical values also shows that for all the beams tested, the ACI (ACI-318-2005) values are generally higher than the CSA (CAN3-A23.3-94 1994) values.

3.1 Cracking moment

The analytical evaluation of deflection depends greatly on the cracking moment of the beams. Cracking moment is usually estimated using the modulus of rupture as:
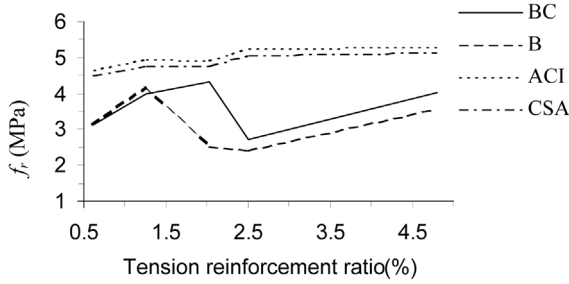
$$M_{cr} = \frac{f_r \cdot I_g}{y_t} \tag{2}$$

A. A. Maghsoudi and H. Akbarzadeh Bengar

Fig. 3(a) The comparison between experimental and theoretical values of f_r with variable ρ for the tested beams of group 1
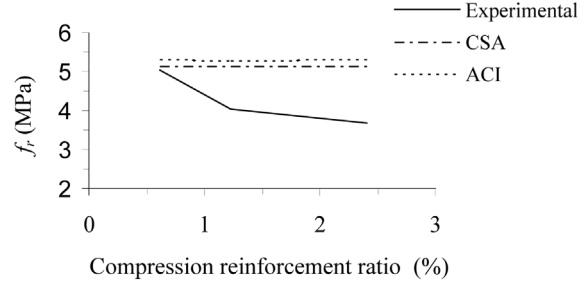
Fig. 3(b) The comparison between experimental and theoretical values of f_r with variable ρ' for the tested beams of group 2

where

f_r = the modulus of rupture and their different values for the two Codes are presented as:

$$f_r = 0.62\sqrt{f_c'} \text{ MPa (ACI) and } f_r = 0.6\lambda\sqrt{f_c'} \text{ MPa (CSA).}$$

Where λ is unity for normal density concrete

y_t = the distance from the neutral axis to the extreme tensile fiber of the beam

The value of f_r usually depends on several factors such as crack observation technique, sensitivity to residual stresses, etc., but here the experimental cracking moment, $M_{cr(exp)}$, is used to determine the experimental cracking stress, $f_{r(exp)}$. The value of $f_{r(exp)}$ versus variation of tensile and compressive reinforcement ratio are respectively shown in Figs. 3(a) and 3(b). Fig. 3 indicates that the experimental cracking stress for the doubly reinforced beams is more than the singly reinforced beams. It also shows that the experimental cracking stresses are less than the values predicted by CSA and ACI.

3.2 Neutral axis depth

The experimental variation of the neutral axis, (N.A.) depth "X" in the constant moment zone is shown in Fig. 4 and Table 4. The depth "X" is obtained from the strain distribution that was measured experimentally in the concrete and the tension reinforcement. In the figure, the horizontal plateau shows that the depth of "X" does not vary between cracking and yielding levels. The results also show that (Fig. 4(a)), by adding ρ' to the singly reinforced beams, the depth of "X" at ultimate state is decreased. The comparison between the ratio of X/d versus loads for singly and doubly reinforced tested beams are also presented in Figs. 4(b),(c). It is clear from Figs. 4(b),(c) and Table 4 that, by increasing the amount of ρ, the values of "X" is increased both for yield and ultimate conditions. Fig. 4(d) is indicated that, by increasing amount of ρ', the depth "X" at both yield and ultimate states is decreased.

3.3 Cracked moment of inertia

The calculation of deflection depends basically on the fully cracked moment of inertia, I_{cr}. The experimental cracked moment of inertia based on the elastic deformation theory is obtained by considering:
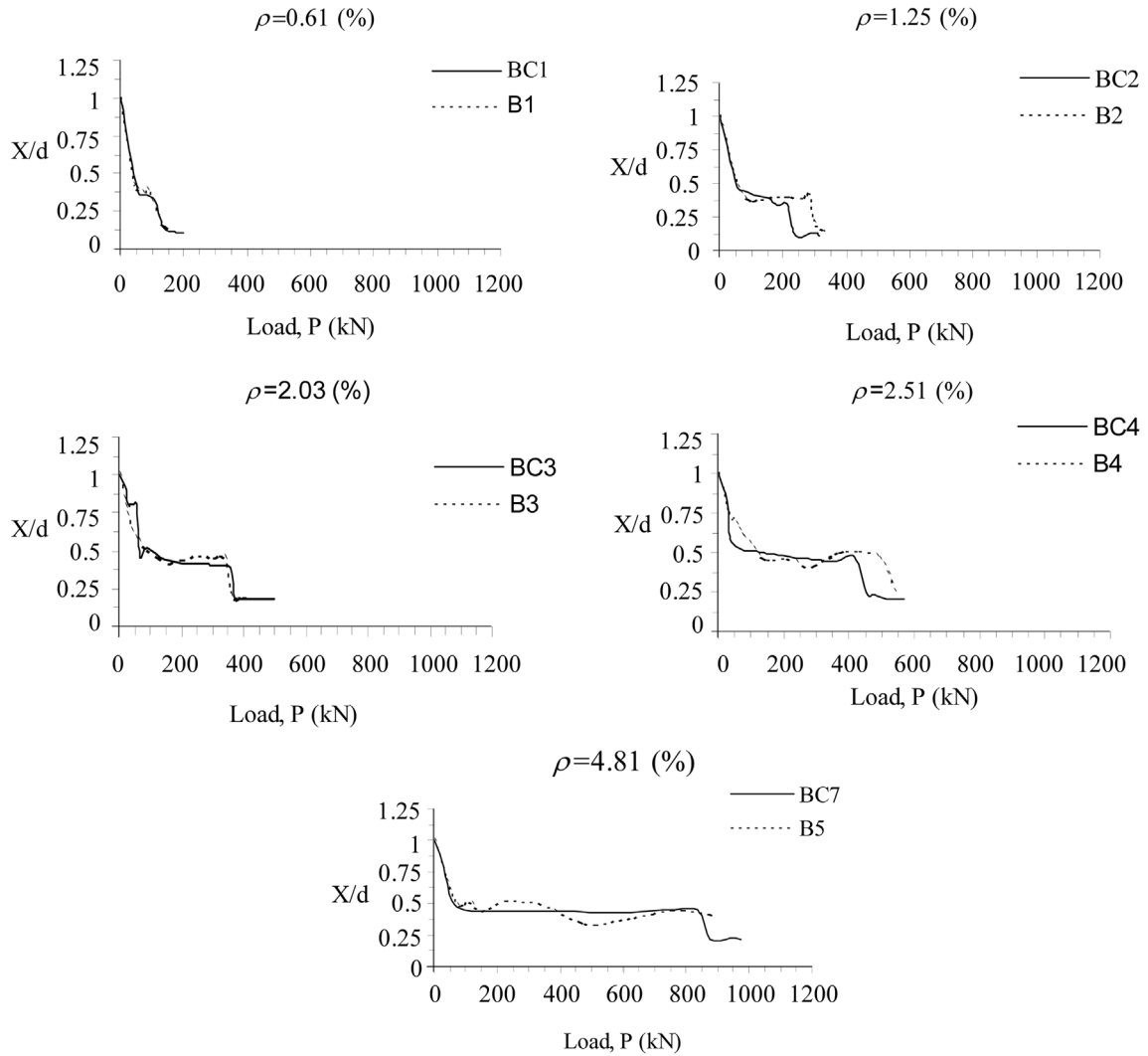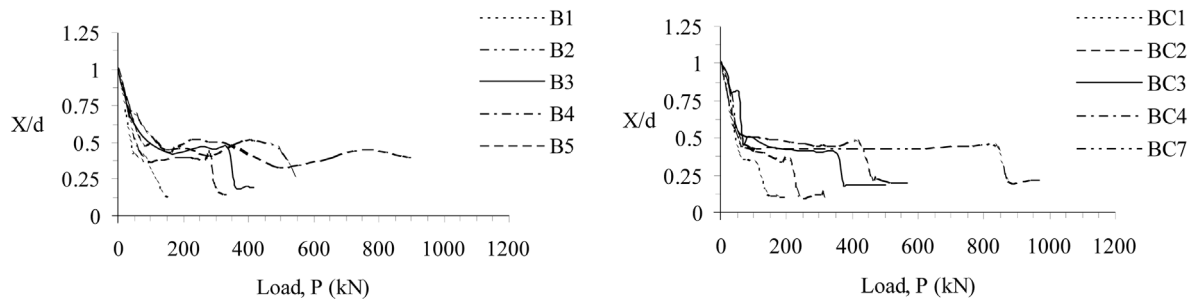
ρ=0.61 (%)

ρ=1.25 (%)

ρ=2.03 (%)

ρ=2.51 (%)

ρ=4.81 (%)

Fig. 4(a) Quality effect of ρ' on behavior of neutral axis depth for beams in group 1

Fig. 4(b) Comparison of neutral axis depth for singly reinforced beams of group 1

Fig. 4(c) Comparison of neutral axis depth for doubly reinforced beams of group 1
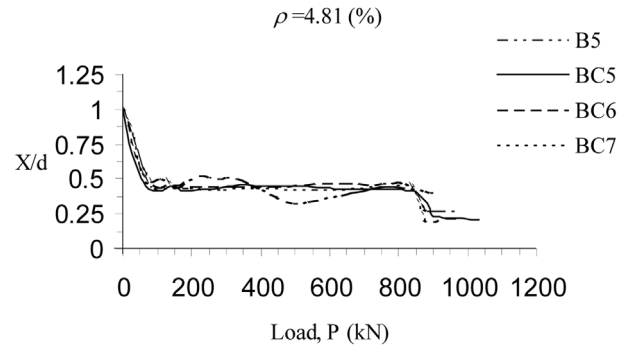
Fig. 4(d) Quantity effect of ρ' on behavior of neutral axis depth for beams in group 2

Table 4 Experimental neutral axis depth at cracking, yield and ultimate
points of Fig. 4

Beam no.	X_{cr} (cm)	X_y (cm)	X_u (cm)
BC1	10.00	8.27	2.70
B1	10.80	10.00	3.00
BC2	11.56	8.77	2.72
B2	12.00	10.00	3.700
BC3	14.10	9.86	4.02
B3	17.20	11.50	4.90
BC4	17.50	11.85	5.20
B4	18.70	12.80	6.50
BC5	19.44	10.78	5.61
B5	15.95	10.56	10.25
BC6	19.88	12.18	5.30
BC7	20.34	11.38	4.82

$$I_{cr(exp1)} = \frac{P_y \cdot a(3l^2 - 4a^2)}{48E_c\Delta_{exp}} \tag{3}$$

where
P_y = the load that causes yielding in the steel reinforcement
a = the shear arm
l = the clear span of the beam
I_{cr} can also be defined as the slope of the line connecting the origin and point of initial yielding of tensile reinforcement in moment curvature curve (Ghali 1993, Macgregor 1988). This is given as:
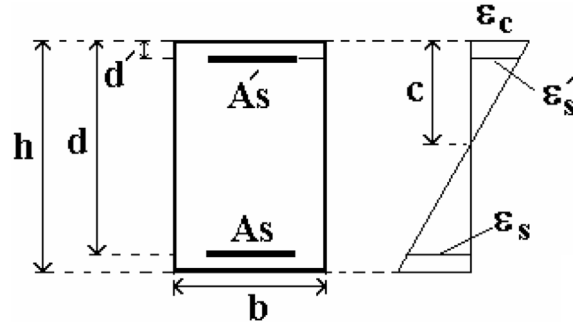
$$I_{cr(exp2)} = \frac{M_y}{E_c\phi_y} \tag{4}$$

Fig. 5 Beam cross section and strain distribution

where

$$\phi_y = \frac{\varepsilon_{cy} + \varepsilon_{sy}}{d} = \frac{\varepsilon_{sy}}{c}$$

ε_{cy} = the measured compression strain in the concrete at yielding of steel reinforcement
ε_{sy} = the measured tensile strain in steel reinforcement at yielding stage
c = neutral axis depth (see Fig. 5)
d = effective depth of the beam

The traditional theoretical definition of I_{cr} based on the cracked transformed section can be given as:
  (a) Beams with singly reinforcement

$$\frac{bc^2}{2} + nA_s c - nA_s d = 0 \tag{5}$$

$$I_{cr} = \frac{bc^3}{3} + nA_s(d - c)^2 \tag{6}$$

  (b) Beams with doubly reinforced

$$\frac{bc^2}{2} + (A_s + A_s')nc - (A_s d + A_s' d')n - A_s'(c - d') = 0 \tag{7}$$

$$I_{cr} = \frac{bc^3}{2} + nA_s(d - c)^2 + (n - 1)A_s'(c - d')^2 \tag{8}$$

where n = E_s/E_c and $E_c = 3200\sqrt{f_c'} + 6900$ (MPa)
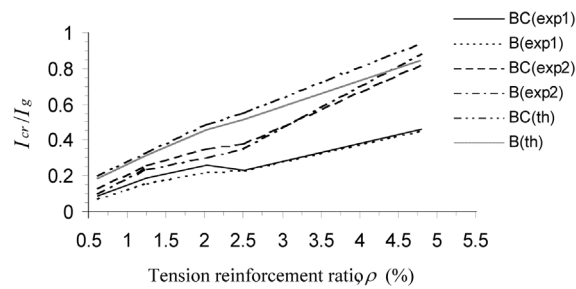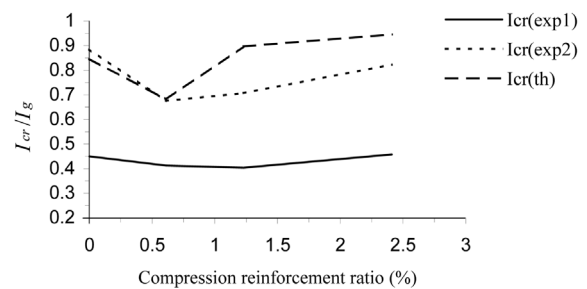 b = width of beam
    d' = cover to compressive bars
    A_s = area of tensile bars
    A_s' = area of compressive bars

Table 5 Theoretical and experimental cracked moment of inertia

Beam no.	$I_{cr(th)} \times 10^6$ (mm^4)	$I_{cr(exp1)} \times 10^6$ (mm^4)	$I_{cr(exp2)} \times 10^6$ (mm^4)
BC1	90.66	38.54	57.68
B1	84.05	33.77	44.31
BC2	150.23	83.00	117.42
B2	143.78	72.18	107.11
BC3	220.93	116.88	157.81
B3	206.38	101.88	134.39
BC4	248.76	104.63	172.57
B4	234.67	104.24	159.76
BC5	390.64	185.48	303.81
B5	381.15	202.52	398.46
BC6	403.63	181.55	317.86
BC7	425.68	205.87	370.31

Fig. 6(a) Effect of ρ on the I_{cr} for the tested beams of group 1

Fig. 6(b) Effect of ρ' on the I_{cr} for the tested beams of group 2

The results of the theoretical and experimental moment of inertia of cracked section are presented in Table 5. It is clear that, for all the cases, the values of $I_{cr(exp)}$ are lower than the values of $I_{cr(th)}$. Also, $I_{cr(exp2)}$ is higher than $I_{cr(exp1)}$. The difference in values of $I_{cr(exp1)}$ and $I_{cr(exp2)}$ is expected due to the great variation in curvature distribution along the beam especially due to the peaks in curvature at the cracks location. Based on this, the graphical representation of I_{cr}/I_g for both the theoretical and experimental values versus ρ and ρ' are shown in Fig. 6. By increasing the percentage of ρ, the value of I_{cr} is increased, such an increase is not highlighted for the beams with amount of ρ greater than 2.0% (Fig. 6a). Also, by comparing the test results of beams, BC, with the beams, B, for either experimental or theoretical values, it is obvious that although ρ' is a variable in BC-beams, the values I_{cr} of BC-beams are higher than that of the B-beams, but the increased amount is small (Fig. 6a). From Fig. 6(b) it is clear that, by increasing the quantity of ρ', the variation in value of I_{cr} is not pronounced.

3.4 Ductility

Ductility is the capacity to undergo inelastic deformation and absorb energy. Several forms of

ductility are often considered (Maghsoudi 1996). These include curvature, rotational and displacement ductility. In this research, displacement ductility and curvature ductility are investigated.
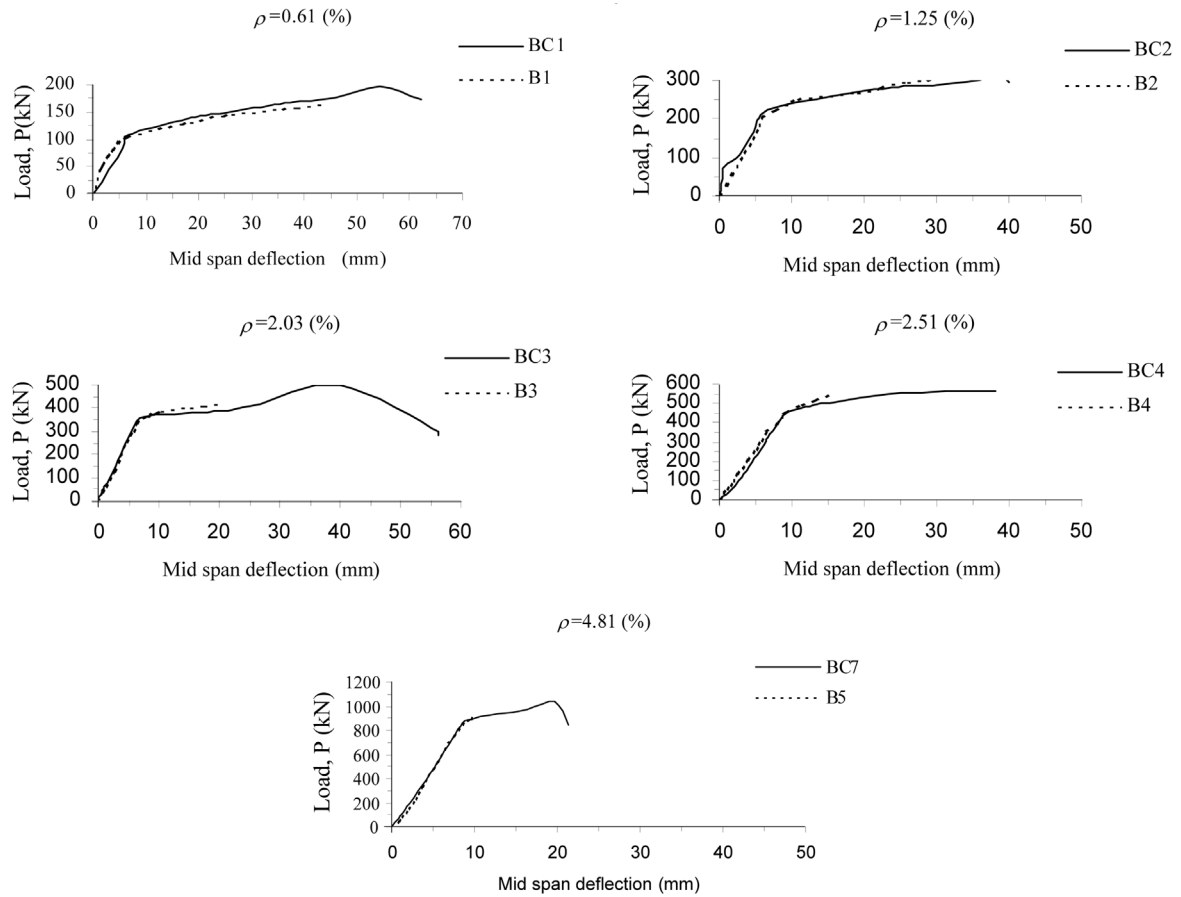

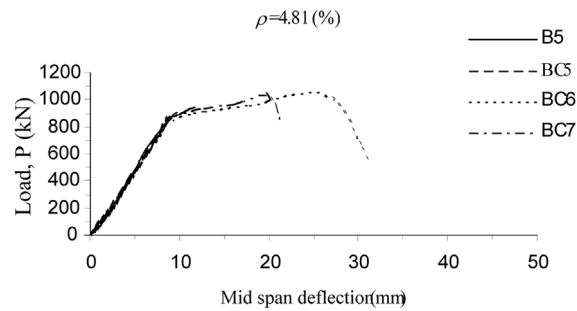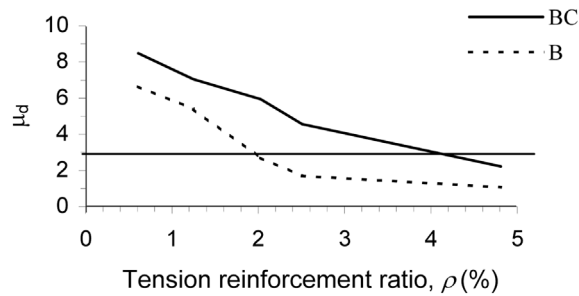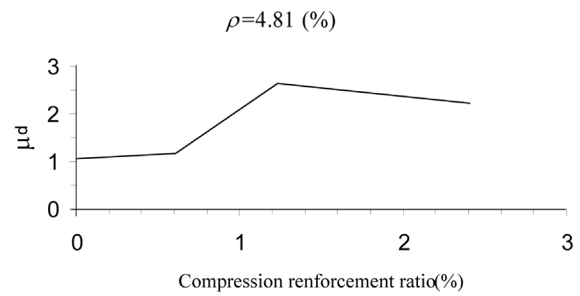Fig. 7(a) Load-deflection beams diagrams for group 1

Fig. 7(b) Load-deflection beams diagrams for group 2

A. A. Maghsoudi and H. Akbarzadeh Bengar

Table 6 Deflection ductility of tested beams

Beam no.	Δ_y (mm)	Δ_u (mm)	$\mu_d = \Delta_u / \Delta_y$
BC1	6.40	54.30	8.48
B1	6.50	43.18	6.64
BC2	5.60	39.40	7.04
B2	5.99	32.40	5.41
BC3	6.73	40.04	5.95
B3	7.40	20.01	2.70
BC4	8.37	38.21	4.56
B4	8.91	15.04	1.69
BC5	10.07	11.93	1.18
B5	9.15	9.7	1.06
BC6	10.03	26.4	2.63
BC7	8.88	19.7	2.218

Fig. 8(a) Effect of ρ on displacement ductility, μ_d, for group 1

Fig. 8(b) Effect of ρ' on displacement ductility, μ_d, for group 2

3.4.1 Displacement ductility

Displacement ductility is defined as the ratio of deflection at ultimate load, Δ_u, to the deflection at first yielding of tensile steel, Δ_y. Ultimate load is the maximum load applied for a beam during testing (Ahmad and Barker 1991, Paster *et al.* 1984).

In Fig. 7 the load deflection curves for two group of beams are presented. Table 6 presents the value of deflections at yielding of tensile reinforcement, Δ_y, and at ultimate load, Δ_u. From results of Fig. 7(a) and Table 6, it is clear that, Δ_u increases as ρ decreases. Also, by adding ρ' in a section, Δ_u will increase. It is obvious that Δ_y increases as ρ increases and Δ_y decreases as ρ' increases in the section. In general, by increasing the quantity of ρ', the ductility Δ_u, was increased.

In Fig. 8, the effect of ρ and ρ' on displacement ductility is presented. As expected, the displacement ductility is decreased as ρ is increased (Fig. 8a). It can also be seen that, by adding ρ', in addition to the moment increase, the ductility will also be increased for HSC beams (see Fig. 8).

A displacement ductility, μ_d, in the range of 3 to 5 is considered imperative for adequate ductility, especially in the areas of seismic design and the redistribution of moments (Ahmad and Barker 1991). Therefore, assuming that a μ_d value of 3 represents an acceptable lower bound to ensuring the ductile behavior of flexural members, it appears that, for the singly reinforced beams with
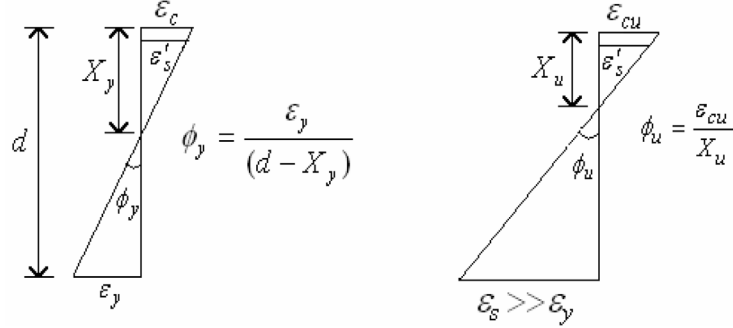
Fig. 9 The strain diagrams at yield and ultimate loads

reinforcement ratios ρ greater than 2.0% would not meet that requirement (Fig. 8a). Whereas, for doubly reinforced beams the ratio of ρ can be increased even up to 4%.

3.4.2 Curvature ductility

Perhaps the most simple and general definition for ductility is defined as the curvature ductility (Maghsoudi 1996). For design, the usual equations for the curvatures at yield load (ϕ_y) and at ultimate (ϕ_u) load (see Fig. 9) are:

(a) Beams with Singly reinforced

$$\phi_y = \frac{f_y}{E_s d(1 - K)} \tag{9}$$

$$K = -\rho n + [2\rho n + \rho^2 n^2]^{1/2} \tag{10}$$

$$\phi_u = \frac{\varepsilon_{cu}}{X_u} \tag{11}$$

$$X_u = \frac{\rho f_y d}{\alpha \beta_1 f_c'} \tag{12}$$

$$\mu_\phi = \frac{\phi_u}{\phi_y} = \frac{\varepsilon_{cu}(\alpha \beta_1 f_c')E_s(1 + \rho n - (2\rho n + \rho^2 n^2)^{1/2})}{\rho f_y^2} \tag{13}$$

(b) Beams with Doubly reinforced

$$\phi_y = \frac{f_y}{E_s d(1 - K)} \quad \text{and} \quad \phi_u = \frac{\varepsilon_{cu}}{X_u}$$

$$K = \left[n^2(\rho + \rho')^2 + 2n\left(\rho + \frac{\rho' d'}{d}\right) \right]^{1/2} - n(\rho + \rho') \tag{14}$$

where compression reinforced is yield, used:

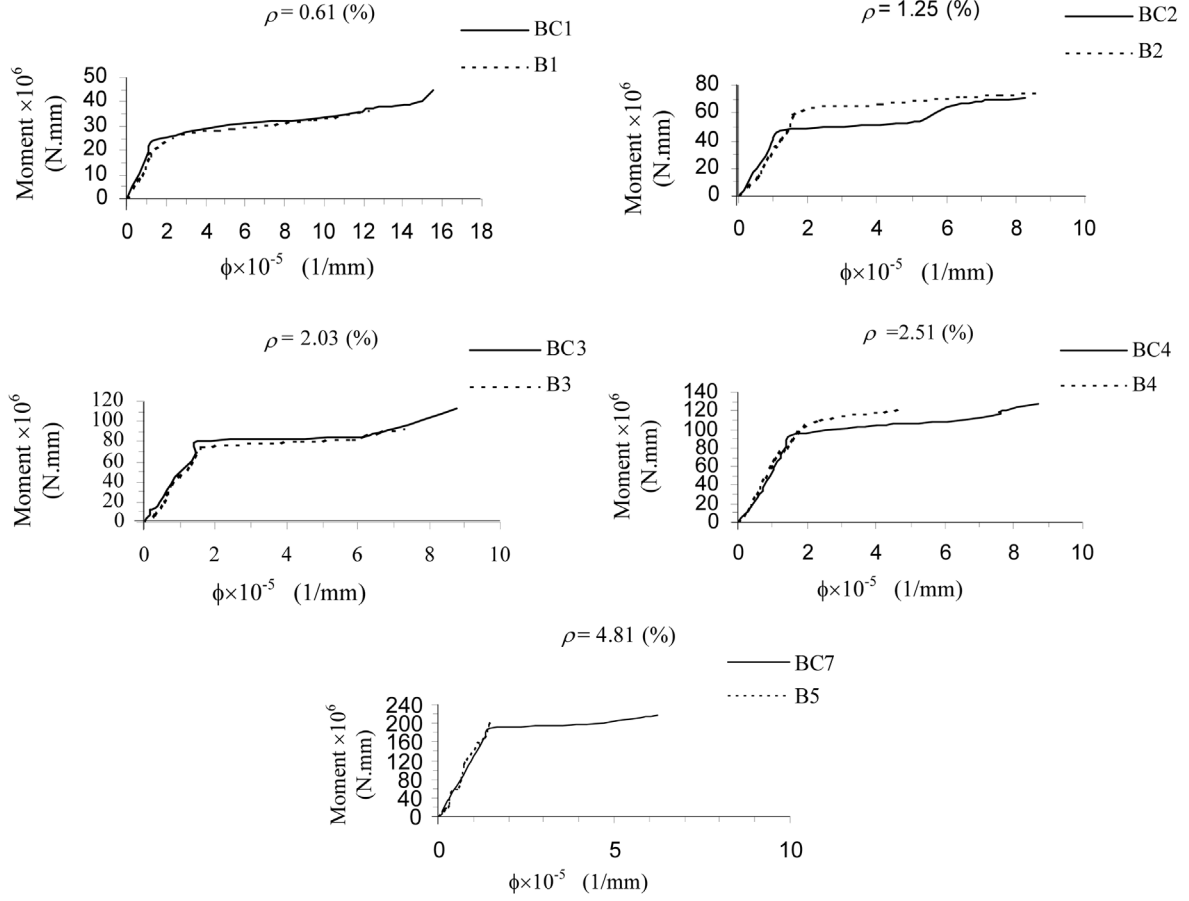$$\phi_u = \varepsilon_{cu} \frac{\alpha \beta_1 f_c' b}{(A_s - A_s')f_y} \tag{15}$$

Fig. 10(a) Mid-span moment-curvature curves for tested beams of group 1

$$\mu = \frac{\alpha\beta_1 f_c' \varepsilon_{cu} E_s}{f_y^2(\rho - \rho')}(1 - K) \tag{16}$$

where compression reinforced is not yield, used:

$$X_u = \left[\frac{(\rho' E_s \varepsilon_{cu} - \rho f_y)^2 d^2}{(2\alpha f_c')^2 \beta_1^2} + \frac{\rho' E_s \varepsilon_{cu} dd'}{(\alpha f_c')\beta_1}\right]^{1/2} - \frac{(\rho' E_s \varepsilon_{cu} - \rho f_y)d}{(2\alpha f_c')\beta_1} \tag{17}$$

$$\mu_\phi = \frac{\phi_u}{\phi_y} = \frac{E_s \varepsilon_{cu}(1 - K)d}{f_y X_u} \tag{18}$$

where
X_u = Neutral axis at ultimate state
X_y = Neutral axis at yielding state
α = the stress block coefficient
β_1 = the ratio between the height of the stress block and X_u
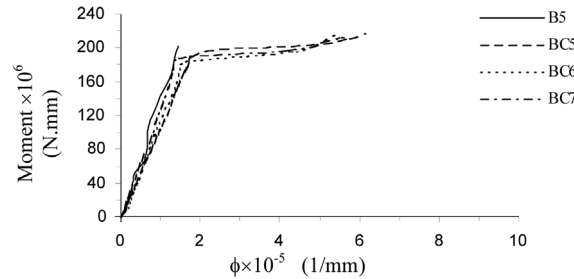E_s = modulus of elasticity of steel

Fig. 10(b) Mid-span moment-curvature curves for tested beams of group 2

Table 7 Comparison of experimental and theoretical curvature ductility

Beam no.	Experimental			Theoretical (ACI)			Theoretical (CSA)		
	$\phi_y \times 10^{-5}$	$\phi_u \times 10^{-5}$	μ_ϕ	$\phi_y \times 10^{-5}$	$\phi_u \times 10^{-5}$	μ_ϕ	$\phi_y \times 10^{-5}$	$\phi_u \times 10^{-5}$	μ_ϕ
BC1	1.31	15.50	11.84	0.98	9.70	9.89	0.98	11.69	11.91
B1	1.20	12.30	10.25	0.98	18.80	19.13	0.98	23.57	23.98
BC2	1.21	8.27	6.84	1.12	7.44	6.68	1.12	9.07	8.13
B2	1.60	8.60	5.38	1.13	9.26	8.22	1.13	11.62	10.31
BC3	1.52	8.75	5.75	1.12	6.20	5.53	1.12	7.71	6.87
B3	1.62	7.33	4.52	1.16	6.17	5.34	1.16	7.69	6.65
BC4	1.55	8.68	5.60	1.25	5.93	4.75	1.25	7.32	5.87
B4	1.71	4.83	2.82	1.31	4.78	3.64	1.31	5.89	4.48
BC5	1.76	5.63	3.20	1.52	2.80	1.84	1.52	3.49	2.29
B5	1.42	1.46	1.03	1.58	2.36	1.50	1.58	2.94	1.86
BC6	1.64	5.40	3.29	1.48	3.18	2.15	1.48	4.01	2.72
BC7	1.44	6.24	4.33	1.41	3.89	2.77	1.41	4.95	3.52

The moment-curvature curves at mid-span sections of tested beams are shown in Fig. 10. For the tested beams, the theoretical and experimental values of ductility at yield and ultimate conditions and also their curvature ductilities are given in Table 7. For both conditions, the values of ϕ_y are increased as ρ increased except for B2, B5 and BC2. By comparing the theoretical and experimental results of beams in group 1, the value of ϕ_y is decreased with the addition of ρ', except for B1 and B5. For all the tested beams (except B5), the amount of $\phi_{y(th)}$ are lower than the $\phi_{y(exp)}$. By increasing ρ, the value of ϕ_u is decreased. Again by comparing the theoretical and experimental result of group 1 beams, the value of ϕ_u is increased when ρ', is added. Considering beams in group 2, the results are indicated that by increasing the quantity of ρ', the value of ϕ_y is decreased whereas the value of ϕ_u is increased.

Almost for all the beams, the $\phi_{u(th)}$ values based on the ACI method (ACI Committee 318 2005), are lower than the $\phi_{u(exp)}$. Whereas, the $\phi_{u(th)}$ based on the CSA method (CAN3-A23.3-94 1994), for the doubly reinforced beams, are lower than the $\phi_{u(exp)}$, but for the singly reinforced beams, these values are higher than the $\phi_{u(exp)}$ values.

The effect of ρ and ρ' on the curvature ductility, μ_ϕ for the tested beams and their theoretical and experimental comparison are plotted in Fig. 11. As can be seen, the theoretical values obtained by
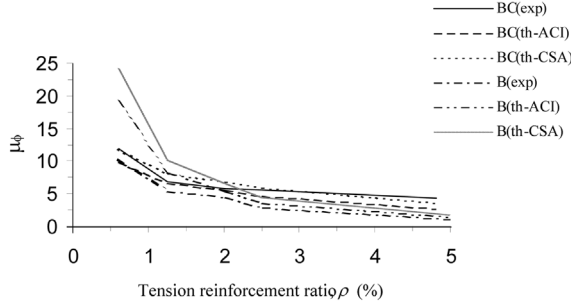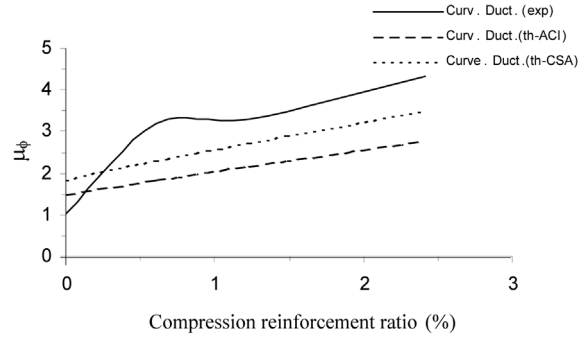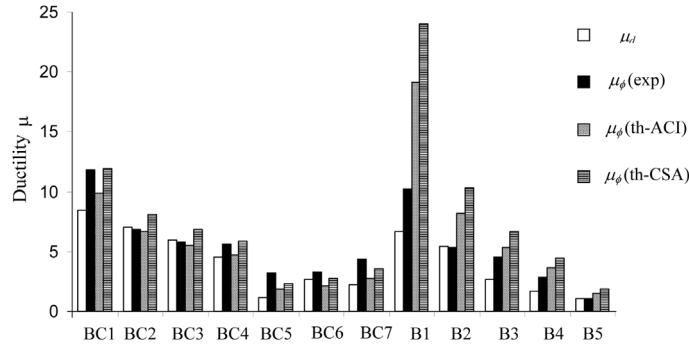
Fig. 11(a) Effect of ρ on curvature ductility, μ_ϕ, for group 1

Fig. 11(b) Effect of ρ' on curvature ductility, μ_ϕ, for group 2

Fig. 12 Comparison of ductility for tested beams

the CSA method are higher than the theoretical values of ACI as well as the experimental results. For the doubly reinforced beams in group 1, having compression reinforcement ρ', for lower percentage of ρ (up to 2.03%), the ACI values are close to the experimental results, whereas for the beams having ρ more than 2.03% the experimental values are close to the CSA. However, for all singly reinforced beams of group 1, the values of $(\mu_\phi)_{exp}$ is lower than the $(\mu_\phi)_{th}$, and the experimental curvature ductility values are close to the ACI values. For beams in group 2, the results of $(\mu_\phi)_{exp}$, are closer to the $(\mu_\phi)_{th}$, based on the CSA.

In Fig. 12 a comparison of displacement ductility for HSC beams with both the theoretical and experimental values of the curvature ductility are presented. The results show that except for beams B1 and BC1 which contained ρ_{min} (0.53%), the difference between the curvature and displacement (both theoretically and experimentally) values of ductility are quite small.

4. Conclusions

The following conclusions can be drawn based on the test results:
1. The experimental cracking stress for the doubly reinforced beams is more than the singly reinforced beams. The experimental cracking stresses are less than the values predicted by CSA and ACI.

2. By increasing the amount of ρ, the N.A. depth is increased both for yield and ultimate conditions. The results also show that, by adding ρ', to the singly reinforced beams, the depth of N.A. at ultimate state is decreased, also by increase amount of ρ' the depth "X" at both yield and ultimate states is decreased.

3. The values of $I_{cr(exp)}$ is lower than the values of $I_{cr(th)}$.

4. Although the use of ρ' in the singly reinforced beams causes an increase in I_{cr}, the increased amount is not significant, also by increasing the quantity of ρ', the variation in value of I_{cr} is not pronounced.

5. For the tested beams, the singly reinforced HSC beams with reinforcement ratios ρ greater than 2.0% the ductility requirement would not be satisfied. However, for doubly reinforced beams the ratio of ρ can be increased even up to 4%.

6. The theoretical curvature ductility values based on the CSA method are higher than the theoretical values of ACI, as well as the experimental results. For the doubly reinforced beams in group 1, having compression reinforcement ρ', for lower percentage of ρ (up to 2.03%), the ACI values are close to the experimental results, whereas for the beams with ρ more than 2.03%, the experimental values are close to the CSA. However, for all singly reinforced beams of group 1, the values of $(\mu_\phi)_{exp}$ is lower than the $(\mu_\phi)_{th.}$, and the experimental curvature ductility values are close to the ACI values. For beams in group 2, the results of $(\mu_\phi)_{exp}$, are closer to the $(\mu_\phi)_{th.}$, based on the CSA.

7. Except for beams B1 and BC1 which contained ρ_{min} (0.53%), the difference between the curvature and displacement (both theoretically and experimentally) values of ductility are quite small.

References

ACI Committee 318 (2005), Building Code Requirements for Structural Concrete and Commentary, American Concrete Institute, ACI 318-02 and ACI 318R-02.

ACI Committee 363 (1992), Review of ACI Code for Possible Revisions for High-Strength Concrete (ACI 362R-92), American Concrete Institute, Detroit.

Ahmad, S.H. and Barker, R. (1991), "Flexural behavior of reinforced high strength lightweight concrete beams", *ACI Mater. J.*, **88**(1), 69-77.

Ashour, A.A. (2000), "Effect of compressive strength and tensile reinforcement ratio on flexural behavior of high-strength concrete beams", *Eng. Struct.*, **22**(5), 413-423.

Ashour, S.A. and Wafa, F.F. (1993), "Flexural behavior of high strength fiber reinforced concrete beams", *ACI Struct. J.*, **90**(3), 279-287.

Ashour, A.A., Wafa, F.F. and Kamal, M.I. (2000), "Effect of the concrete compressive strength and tensile reinforcement ratio on the flexural behavior of fibrous concrete beams", *Eng. Struct. J.*, **22**(9), 1133-1146.

CAN3-A23.3-94. (1994), Design of Concrete Structures for Building, Canadian Standards Association, Ontario, Canada.

Ghali, A. (1993), "Deflection of reinforced concrete members, a critical review", *ACI Struct. J.*, **90**(4), 364-373.

Khuntia, M. and Ghosh, S.K. (2004), "Flexural stiffness of reinforced concrete columns and beams", *ACI Struct. J.*, **101**(3), 351-363.

Leslie, K.E., Rajagopalan, K.S. and Everard, N.J. (1976), "Flexural behavior of high-strength concrete beams", *ACI Struct. J.*, **73**(9), 517-521.

Macgregor, I.G. (1988), *Reinforced Concrete Mechanics and Design*, New Jersey, Prentice-Hall International, U.S.A.

Maghsoudi, A.A. (1996), *Design for Ductility of Structures*, Shaheed Bahonar University Publications, Kerman, Iran.

Nilson, A.H. (1987), "Design implication of current research on high strength concrete", High-Strength Concrete, ACI SP-87, American Concrete Institute, Detroit.

Ozbakkaloglu, T. and Saatcioglu, M. (2004), "Rectangular stress block for high-strength concrete", *ACI Struct. J.*, **101**(4), 475-483.

Paster, J.A., Nilson, A.H. and Slate, F.O. (1984), "Behavior of high-strength concrete beams", Report No. 84-3, Department of Structural Engineering, Cornell University, Ithaca, NY.

Shin, S.W., Ghosh, S.K. and Moreno, J. (1989), "Flexural ductility of ultra-high strength concrete members", *ACI Struct. J.*, **86**(9), 394-400.

Swamy, R.N. (1987), "High strength concrete-material properties and structural behavior", High-Strength Concrete, ACI SP-87. American Concrete Institute, Detroit.

Tsong, Y., Yen, L.H. and Jaw, W.T. (1989), "Amelioration of stirrup and compression reinforcement on the ductility of reinforced high-strength concrete beam", *Proc. of the Structures Congress*, San Francisco, CA, May 1-5.